

Anisotropic geometrical-spreading correction for wide-azimuth P-wave reflections

Xiaoxia Xu and Ilya Tsvankin

**Colorado School of Mines, Department of Geophysics, Center for Wave
Phenomena, Golden, CO 80401-1887, USA**

(February 8, 2006)

ABSTRACT

Compensation for the geometrical spreading along the raypath is one of the key steps in AVO (amplitude variation with offset) analysis, in particular for wide-azimuth surveys. Here, we propose an efficient methodology to correct long-spread, wide-azimuth reflection data for the geometrical spreading in stratified azimuthally anisotropic media. The P-wave geometrical-spreading factor is expressed through the reflection traveltimes described by a nonhyperbolic moveout equation that has the same form as in VTI (transversely isotropic with a vertical symmetry axis) media.

The adapted VTI equation is parameterized by the normal-moveout (NMO) ellipse and the azimuthally varying anellipticity parameter $\eta(\alpha)$. To estimate the moveout parameters, we apply the 3D nonhyperbolic semblance algorithm of Vasconcelos and Tsvankin that operates simultaneously with traces at all offsets and azimuths. The estimated moveout parameters are used as the input in the geometrical-spreading computation. Numerical tests for models composed of orthorhombic layers with strong, depth-varying velocity anisotropy confirm the high accuracy of our traveltimes-fitting procedure and, therefore, of the geometrical-spreading correction. Since our algorithm is entirely based on the kinematics of reflection arrivals, it can be readily incorporated into the processing flow of azimuthal AVO analysis.

In combination with the nonhyperbolic moveout inversion, the method was applied

to wide-azimuth P-wave data collected at Weyburn field in Canada. The geometrical-spreading factor for the reflection from the top of the fractured reservoir is clearly influenced by the azimuthal anisotropy in the overburden, which should cause distortions in the azimuthal AVO attributes. This case study confirms that the azimuthal variation of the geometrical-spreading factor is often comparable to or exceeds that of the reflection coefficient.

INTRODUCTION

Seismic signatures measured in wide-azimuth reflection surveys may be strongly influenced by azimuthal anisotropy associated with natural fracture systems, nonhydrostatic stresses, or dipping transversely isotropic layers (e.g., shales). The inversion of azimuthally varying traveltimes and amplitudes of reflected waves gives valuable information for characterization of fractured reservoirs and lithology discrimination (Mallick et al., 1998; Grechka and Tsvankin, 1999a; Lynn et al., 1999; Bakulin et al., 2000; Rüger, 2001; Hall and Kendall, 2003). Although the most direct evidence of the presence of azimuthal anisotropy is provided by shear-wave splitting, estimation of a representative set of anisotropic parameters is impossible without performing azimuthal moveout and/or amplitude-variation-with-offset (AVO) analysis.

The main advantages of the anisotropic AVO inversion are the possibility to resolve the reflection coefficient at the target horizon and the high sensitivity of body-wave reflectivity to the anisotropic parameters (e.g., Tsvankin, 1995, 2005; Rüger, 2001). However, the transformation of seismic amplitudes measured at the surface into the reflection coefficients involves corrections for the source signature and propagation phenomena along the raypath (e.g., Maultzsch et al., 2003). Major amplitude distortions in anisotropic media, in particular for wide-azimuth data, are caused by the directionally varying geometrical spreading above the reflector. A detailed discussion of geometrical spreading in TI and orthorhombic media can be found in Ursin and

Hokstad (2003), Tsvankin (2005, Chapter 2) and Xu et al. (2005; hereafter referred to as Paper I).

If the velocity model of the overburden is known, geometrical spreading can be computed, for example, by performing dynamic ray tracing. A more practical approach, however, is based on expressing geometrical spreading through reflection traveltimes using ray theory (e.g., see equation 4.10.50 in Červený, 2001). As shown in Paper I, the geometrical-spreading factor L for laterally homogeneous media can be found as the following function of traveltime T :

$$L(x, \alpha) = \frac{\sqrt{\cos \phi^s \cos \phi^r}}{V_g} \left[\frac{\partial^2 T}{\partial x^2} \frac{\partial T}{\partial x} \frac{1}{x} + \frac{\partial^2 T}{\partial x^2} \frac{\partial^2 T}{\partial \alpha^2} \frac{1}{x^2} - \left(\frac{\partial T}{\partial \alpha} \right)^2 \frac{1}{x^4} \right]^{-1/2}, \quad (1)$$

where x is the source-receiver offset, α is the azimuth of the source-receiver line with respect to the x_1 -axis, V_g is the group velocity at the source location, and ϕ^s and ϕ^r are the angles between the ray and the vertical at the source and receiver, respectively.

In Paper I, equation 1 is combined with the Tsvankin-Thomsen (1994) nonhyperbolic moveout equation for the traveltime T to study the P-wave geometrical spreading in a horizontal orthorhombic layer. Analytic results and numerical modeling reveal pronounced distortions of the geometrical spreading caused by both polar and azimuthal anisotropy. Paper I demonstrates that reliable recovery of the reflection coefficient from the azimuthal AVO response often requires an accurate anisotropic geometrical-spreading correction (also, see Mallick et al., 1998).

The goal of this paper is to develop a practical implementation of the geometrical-spreading correction for layered azimuthally anisotropic media. The main emphasis of the paper is on models with orthorhombic symmetry considered typical for naturally fractured reservoirs (e.g., Schoenberg and Helbig, 1997; Bakulin et al., 2000). It is clear from equation 1 that the key issue in computing the geometrical-spreading factor from surface data is to find a smooth approximation for reflection traveltime that can be used for a wide range of offsets and azimuths.

We start by testing the accuracy of a simplified P-wave moveout equation based

on the approximate kinematic equivalence between orthorhombic and VTI media. While this equation provides a good fit to the traveltimes for layered models with a uniform (identical) orientation of the vertical symmetry planes in all layers, it requires modification when the symmetry-plane azimuths vary with depth. We use the 3D semblance algorithm of Vasconcelos and Tsvankin (2004) to estimate the best-fit moveout parameters needed to evaluate the traveltime derivatives in equation 1. Numerical tests for layered orthorhombic models confirm that azimuthal anisotropy may produce comparable distortions in the geometrical spreading and in the reflection coefficient. Finally, we apply the algorithm to wide-azimuth data collected at Weyburn field in Canada to evaluate the azimuthally varying geometrical-spreading factor for wide-angle reflections from the reservoir.

MOVEOUT EQUATIONS FOR ORTHORHOMBIC MEDIA

Homogeneous layer

The analysis in Paper I confirms the conclusion of Al-Dajani et al. (1998) that P-wave reflection traveltime in a horizontal orthorhombic layer with a horizontal symmetry plane is well-described by the Tsvankin-Thomsen (1994) nonhyperbolic moveout equation. The form of this equation remains the same for different anisotropic symmetries, but in the presence of azimuthal anisotropy the moveout coefficients become azimuthally dependent:

$$T^2(x, \alpha) = T_0^2 + \frac{x^2}{V_{\text{nmo}}^2(\alpha)} + \frac{A_4(\alpha) x^4}{1 + A(\alpha) x^2}. \quad (2)$$

Here, V_{nmo} is the normal-moveout (NMO) velocity, A_4 is the quartic moveout coefficient, and A is the coefficient that ensures the convergence of equation 2 for large source-receiver offsets.

The azimuthally varying NMO velocity traces out an ellipse with the axes parallel to the vertical symmetry planes of the orthorhombic layer (Grechka and Tsvankin,

1998):

$$V_{\text{nmo}}^{-2}(\alpha) = \frac{\sin^2(\alpha - \phi)}{\left(V_{\text{nmo}}^{(1)}\right)^2} + \frac{\cos^2(\alpha - \phi)}{\left(V_{\text{nmo}}^{(2)}\right)^2}, \quad (3)$$

where $V_{\text{nmo}}^{(1)}$ and $V_{\text{nmo}}^{(2)}$ are the semi-minor and semi-major axes of the NMO ellipse, respectively, and ϕ is the azimuth of the semi-major axis.

Explicit expressions for the coefficients $A_4(\alpha)$ and $A(\alpha)$ are given in Al-Dajani et al. (1998) and Paper I. However, the nonhyperbolic (x^4) term in equation 2 can be substantially simplified by using an approximate equivalence between the P-wave kinematics in the vertical symmetry planes of orthorhombic and VTI media. The VTI moveout equation of Alkhalifah and Tsvankin (1995) can be adapted for an orthorhombic layer by introducing an azimuthally varying anellipticity coefficient $\eta(\alpha)$ (Pech and Tsvankin, 2004; Paper I):

$$T^2(x, \alpha) = T_0^2 + \frac{x^2}{V_{\text{nmo}}^2(\alpha)} - \frac{2\eta(\alpha) x^4}{V_{\text{nmo}}^2(\alpha) [T_0^2 V_{\text{nmo}}^2(\alpha) + (1 + 2\eta(\alpha)) x^2]}, \quad (4)$$

$$\eta(\alpha) = \eta^{(1)} \sin^2(\alpha - \phi) + \eta^{(2)} \cos^2(\alpha - \phi) - \eta^{(3)} \sin^2(\alpha - \phi) \cos^2(\alpha - \phi). \quad (5)$$

The anellipticity parameters $\eta^{(1)}$, $\eta^{(2)}$, and $\eta^{(3)}$ are defined in the symmetry planes by analogy with the Alkhalifah-Tsvankin parameter η for VTI media (Grechka and Tsvankin, 1999b).

Although the analogy between orthorhombic and VTI media is based on the weak-anisotropy approximation, extensive numerical testing shows that equation 4 with fitted moveout parameters provides excellent accuracy for a homogeneous orthorhombic layer with a horizontal symmetry plane (see also Vasconcelos and Tsvankin, 2004). In Figure 1, the parameters $V_{\text{nmo}}^{(1)}$, $V_{\text{nmo}}^{(2)}$, $\eta^{(1)}$, $\eta^{(2)}$, $\eta^{(3)}$, and ϕ were found by fitting equation 4 to ray-traced traveltimes using the least-squares method. Here and in the examples below, the synthetic data are generated using ANRAY – the 3D anisotropic ray-tracing code of Gajewski and Pšenčík (1990). The difference between the ray-traced traveltimes and those computed from equation 4 is much less than 1% of

the zero-offset two-way traveltime (i.e., less than 4 ms) for a wide range of offsets and azimuths. Note that the model in Figure 1 has substantial polar and azimuthal anisotropy, and the maximum offset-to-depth ratio is as large as three. The influence of traveltime errors on the computation of the moveout parameters and geometrical spreading is analyzed in detail below.

Layered models with uniform symmetry-plane orientation

Next, we apply equation 4 to more complicated, multilayered azimuthally anisotropic models. Suppose the medium above the reflector includes horizontal layers of orthorhombic or higher symmetries, and the vertical symmetry planes in each layer have the same orientation. Note that in azimuthally isotropic (i.e., VTI or purely isotropic) media any vertical plane is a plane of mirror symmetry. The uniform orientation of the symmetry planes in all layers implies that the model as a whole has two orthogonal vertical symmetry planes.

Because of the kinematic equivalence between the symmetry planes of orthorhombic and VTI media, P-wave nonhyperbolic moveout in the symmetry-plane directions is well-described by equation 4 with the effective parameter η computed from the VTI averaging equations (Tsvankin, 1997; 2005, Appendix 4B). Although for off-symmetry azimuthal directions the kinematic analogy with VTI media is valid only for weak anisotropy, the numerical testing in the last section indicates that equation 4 parameterized by the best-fit values of V_{mmo} and η may be sufficiently accurate for any given azimuth. It is not clear, however, whether or not the azimuthal variation of the effective parameter $\eta(\alpha)$ can be described by the single-layer equation 5.

To estimate the effective moveout parameters in equation 4 without traveltime picking, we employ the 3D nonhyperbolic semblance algorithm of Vasconcelos and Tsvankin (2004). They developed a three-step procedure designed to make the multiparameter semblance search for wide-azimuth surveys more efficient. First,

conventional-spread data are used to reconstruct the NMO ellipse and estimate the symmetry-plane azimuth ϕ and the NMO velocities $V_{\text{nmo}}^{(1)}$ and $V_{\text{nmo}}^{(2)}$. Second, the anellipticity parameters $\eta^{(1)}$ and $\eta^{(2)}$, which are defined in the vertical symmetry planes, are found from the VTI nonhyperbolic semblance analysis in narrow sectors centered at the symmetry-plane directions. The third step is a full-azimuth nonhyperbolic semblance search based on equations 3–5, with the estimated values of the parameters ϕ , $V_{\text{nmo}}^{(1)}$, $V_{\text{nmo}}^{(2)}$, $\eta^{(1)}$, and $\eta^{(2)}$ used to specify the starting model.

Application of this semblance algorithm to ray-traced seismograms computed for the four-layer model with the parameters listed in Table 1 confirms that equation 4 accurately describes long-spread moveout for the full range of azimuths (Figure 2). The model includes two orthorhombic layers with a substantial magnitude of polar and azimuthal anisotropy sandwiched between two isotropic layers. The error of equation 4 does not exceed 0.3% of the zero-offset traveltimes for all offsets and azimuths; similar results were obtained for a wide range of plausible orthorhombic models.

The high accuracy of the traveltimes fitting method, however, does not imply that the estimated effective NMO velocity and, especially, the coefficient η are always close to the analytic values because of the tradeoffs between various moveout parameters (Vasconcelos and Tsvankin, 2004). Nevertheless, as long as equation 4 accurately matches the exact traveltimes, the best-fit moveout parameters provide suitable input for the geometrical-spreading correction.

Models with misaligned symmetry planes

For media without throughgoing vertical symmetry planes, the azimuthal variation of the quartic moveout coefficient A_4 becomes more complicated (Al-Dajani et al., 1998), and equation 5 for the parameter η may no longer be accurate. However, extensive testing that we performed for a range of orthorhombic models with misaligned symmetry planes shows that traveltimes errors seldom exceed 0.5% of the

zero-offset time. Apparently, the magnitude of the additional terms in the azimuthal dependence of η is relatively small, and the moveout-inversion algorithm compensates for these missing terms by adjusting the best-fit parameters $\eta^{(1)}$, $\eta^{(2)}$, and $\eta^{(3)}$.

Model 2 used in Figure 3 contains two orthorhombic layers with uncommonly large values of the anisotropy parameters and the vertical symmetry planes misaligned by 45° (Table 2). For this extreme example, the normalized errors of equation 4 reach 1%. While traveltimes errors on the order of 0.5–1% may be acceptable for purposes of conventional moveout inversion, they propagate with amplification into the geometrical-spreading factor (equation 1).

To improve time fitting for multilayered anisotropic media with misaligned symmetry planes, equation 5 can be modified in a relatively straightforward way. To introduce this modification, we analyze the effective parameter $\eta(\alpha)$ for a stack of horizontal orthorhombic layers by applying the VTI averaging equation (Tsvankin, 2005, equation 4.47) for each azimuth α :

$$\eta(\alpha) = \frac{1}{8} \left\{ \frac{1}{V_{\text{nm0}}^4(\alpha) T_0} \left[\sum_{i=1}^N (V_{\text{nm0}}^{(i)}(\alpha))^4 (1 + 8\eta^{(i)}(\alpha)) T_0^{(i)} \right] - 1 \right\}, \quad (6)$$

where $V_{\text{nm0}}^{(i)}(\alpha)$ and $\eta^{(i)}(\alpha)$ are the interval parameters in layer i . Although equation 6 may become inaccurate for models with strong azimuthal anisotropy, it usually reproduces the shape of the azimuthal variation of the effective η (Al-Dajani et al., 1998).

Figure 4 shows a comparison between the parameter η computed from equation 6 (solid curve) and estimated by the moveout-inversion algorithm (dashed) for a two-layer orthorhombic model with the symmetry planes misaligned by 15° . The shape of the two curves is quite similar, which explains the relatively low magnitude of the time residuals typically produced by equation 4. The misalignment of the symmetry planes, however, causes a rotation of the estimated η -curve with respect to the one calculated from equation 6.

The moveout-inversion algorithm cannot accommodate this rotation because the

“principal axes” of the azimuthal variation of $\eta(\alpha)$ in equation 5 are parallel to the axes of the NMO ellipse (equation 3). Therefore, the traveltimes fitting at far offsets can be improved by decoupling the nonhyperbolic moveout term from the NMO ellipse and introducing an additional angle ϕ_1 responsible for the azimuthal variation of the effective parameter η :

$$\eta(\alpha) = \eta^{(1)} \sin^2(\alpha - \phi_1) + \eta^{(2)} \cos^2(\alpha - \phi_1) - \eta^{(3)} \sin^2(\alpha - \phi_1) \cos^2(\alpha - \phi_1) \quad (7)$$

The first two steps of the modified moveout-inversion algorithm remain the same as those described above, but at the last step we fix the orientation of the NMO ellipse (angle ϕ) and search for the angle ϕ_1 and the other moveout parameters using the full range of offsets and azimuths. Application of this algorithm to model 2 (Table 2) results in a greatly improved time fitting (compare Figure 5 with Figure 3) and a 15% increase in the total semblance value. Hence, equation 7 helps to make our moveout approximation suitable even for models with uncommonly strong, depth-varying azimuthal anisotropy.

AZIMUTH-DEPENDENT GEOMETRICAL-SPREADING CORRECTION

The traveltimes derivatives in the geometrical-spreading equation 1 can be computed from the best-fit moveout parameters in equation 4. Explicit expressions for these derivatives are given in Appendix A.

Equation 1 also contains the group angles at the source (ϕ^s) and receiver (ϕ^r) locations. Since our model is laterally homogeneous, the ray parameter (horizontal slowness) p_{hor} does not change along the raypath and can be computed as

$$p_{\text{hor}} = \sqrt{\left(\frac{\partial T}{\partial x}\right)^2 + \left(\frac{1}{x} \frac{\partial T}{\partial \alpha}\right)^2} \quad (8)$$

In most cases of practical importance, the subsurface layer is isotropic and has a known P-wave velocity V . Then the group angles at the source and receiver can be

found directly from p_{hor} :

$$\cos \phi^s = \cos \phi^r = \sqrt{1 - p_{\text{hor}}^2 V^2} . \quad (9)$$

If the subsurface layer is anisotropic, estimation of the group angles from the travel-time derivatives involves the relevant anisotropy parameters.

Combining equation 1 with the expressions in Appendix A and taking equation 9 into account, one can compute the geometrical spreading from the best-fit moveout parameters.

Synthetic example

Using the method described above, we calculated the geometrical-spreading factor $L(x, \alpha)$ for the reflection from the bottom of layer 3 in model 1 (Table 1). As was the case for the homogeneous orthorhombic medium discussed in Paper I, the influence of anisotropy leads to pronounced, azimuthally-dependent distortions of the geometrical spreading (Figure 6). For an offset-to-depth-ratio of unity, the factor L decreases by 17% between the azimuths $\alpha = 0^\circ$ and 90° (Figure 7). Since all layers are horizontal, the dependence of the geometrical spreading on azimuth is caused entirely by the azimuthal anisotropy above the reflector. For comparison, the azimuthal variation of the reflection coefficient for the same event is less than 13% (Figure 8). Clearly, if the anisotropic geometrical spreading is unaccounted for, it can compromise the azimuthal AVO signature for this model.

The high accuracy of our algorithm is verified by comparing its output with the results of dynamic ray tracing (Figure 9). The geometrical-spreading factors computed by the two methods are almost identical for offset-to-depth ratios less than 1.5, and only slightly diverge at longer offsets. The deviation of our result from that of the ray tracing, which reaches a maximum of 6% for $\alpha = 0^\circ$, can be explained by the approximate nature of equation 4 and, possibly, by numerical errors in both algo-

rithms. Overall, our method produces a sufficiently accurate geometrical-spreading factor in layered orthorhombic media for a wide range of offsets and azimuths.

Error analysis

To study the influence of realistic traveltimes noise on the geometrical spreading computed by our method, we added linear and sinusoidal time errors to the reflection traveltimes for model 1 (Table 1 and Figure 2). Linear traveltimes noise can approximate long-period static errors, whereas sinusoidal errors can be due to short-period statics.

The linear time error changes from 4 ms at zero offset to -4 ms at the maximum offset (equal to two reflector depths) for each azimuth α . Application of our algorithm to the perturbed traveltimes in the full range of azimuths yields slightly distorted values of the velocities $V_{\text{nmo}}^{(1,2)}$ (the errors are about 1%) and parameters $\eta^{(1,2,3)}$ (the errors are less than 0.03); the maximum error in the geometrical spreading does not exceed 2%. When the magnitude of the linear error function increases from 4 ms to 8 ms, the corresponding geometrical-spreading error reaches only 5%. It is noteworthy that the moveout parameters estimated from wide-azimuth data are less sensitive to linear traveltimes errors than those obtained from 2D semblance analysis for VTI media (Tsvankin, 2005). On the whole, our geometrical-spreading computation is sufficiently robust in the presence of moderate linear noise.

To test the influence of short-period static errors, the traveltimes for model 1 were contaminated by several sinusoidal functions of the form $A \sin(n\pi x/x_{\text{max}}) \sin m\alpha$. The maximum time error A was fixed at 4 ms; the coefficients n and m control the period of the error function in the radial and azimuthal directions, respectively. When $m = 0$ (i.e., no azimuthal variation in the error) and n is an even number, the spreading remains almost unchanged. Apparently, an equal number of peaks and troughs over the spreadlength compensate for one another, and the noise does not noticeably distort

the best-fit moveout parameters and, consequently, the geometrical spreading. However, when n is an odd number (i.e., the number of peaks and troughs differs by one), the sinusoidal error does influence the output of our algorithm. The most significant distortion in geometrical spreading occurs for $n = 3$, when the maximum spreading error reaches 4% (for $m = 0$) over the whole range of offsets and azimuths; the error decreases with n .

Next, we make the traveltime error azimuthally dependent by varying m . Our tests show that the spreading errors are higher when m is an even number because in this case the azimuthal variation of the error function is similar to that of the traveltime $T(x, \alpha)$, which is governed by $\sin^2 \alpha$ and $\cos^2 \alpha$ [see equations 3–5]. Figure 10 displays the distortion in the geometrical spreading caused by the error function $4 \sin(3\pi x/x_{\max}) \sin 4\alpha$ (i.e., $n = 3$ and $m = 4$). The maximum error of just 4% is the same as the one that was obtained for the azimuthally invariant error function with $n = 3$. When the magnitude of the error function increases from 4 ms to 8 ms, the corresponding geometrical-spreading error only doubles for fixed values of m and n .

Since it is difficult to study the influence of all plausible traveltime distortions (obviously, not limited to statics errors) on the geometrical spreading, next we examine the sensitivity of the factor L to errors in the input moveout parameters (see Appendix A). The geometrical-spreading error in a symmetry plane of model 1 caused by Gaussian noise added to the moveout parameters is shown in Figure 11. The level of this noise is slightly higher than the largest distortions caused by the traveltime errors studied above.

As the offset-to-depth ratio increases from one to two, the standard deviation of the error in L grows from 5% to 8%. Still, given the relatively high level of errors in the input parameters, the distortion of the spreading factor remains acceptable within the practically important offset range of up to two reflector depths. In particular, the geometrical-spreading error is smaller than the percentage error in each moveout parameter when the other parameters are held constant, which indicates that our

operator is sufficiently stable. For example, a 5% error in $V_{\text{nmo}}^{(1)}$ yields an error in L of less than 3% if the offset-to-depth ratio does not exceed two.

Field-data application

To demonstrate the influence of azimuthal anisotropy on the geometrical spreading for field data, we applied the algorithm to wide-azimuth reflection events acquired above a fractured reservoir at Weyburn field in Canada by the Reservoir Characterization Project (a research consortium at CSM). Vasconcelos and Tsvankin (2004) carried out nonhyperbolic moveout inversion for P-wave reflections from several interfaces in the overburden and obtained relatively large values of the parameters $\eta^{(1,2,3)}$ reaching 0.25. They also concluded that at least the shallow part of the overburden exhibits non-negligible azimuthal anisotropy.

These results are in good agreement with the analysis of shear-wave splitting by Cardona (2002) and of the azimuthal AVO response by Jenner (2001). In particular, Jenner (2001) found that the P-wave AVO attributes at the reservoir level vary with azimuth. His amplitude processing, however, included only the conventional geometrical-spreading correction for isotropic media.

To evaluate possible anisotropy-induced distortions of the geometrical spreading, we applied our algorithm to the reflection from the top of the reservoir (Figure 12). The moveout parameters were obtained by Vasconcelos and Tsvankin (2004) using equations 3–5. The influence of anisotropy causes a dramatic 50% distortion in the geometrical spreading for offset-to-depth ratios close to two. The magnitude of the azimuthal variation of the factor L at offset-to-depth ratios slightly larger than unity reaches 10% (Figure 13). Such a difference between the geometrical spreading in the east-west and north-south directions may cause noticeable distortions in the azimuthal variation of the AVO gradient studied by Jenner (2001).

DISCUSSION AND CONCLUSIONS

The formalism suggested in Paper I provides an analytic basis for geometrical-spreading correction in layered azimuthally anisotropic media. Since the correction involves only the spatial derivatives of the reflection traveltime and the group-velocity vector at the source/receiver locations, it does not require knowledge of the velocity field beneath the subsurface layer. The main issue in computing geometrical spreading for purposes of wide-angle azimuthal AVO analysis is to find a sufficiently accurate, smooth approximation for long-offset, multiazimuth reflection moveout in the presence of azimuthal anisotropy.

Numerical testing shows that even for models composed of strongly anisotropic orthorhombic layers, long-spread P-wave reflection traveltime can be accurately described by a nonhyperbolic moveout equation that has the same form as the widely used Alkhalifah-Tsvankin equation for VTI media. Keeping the same general form of the moveout equation for azimuthally anisotropic and VTI media helps to facilitate the transition between models with different symmetries in both the moveout inversion and geometrical-spreading correction. To accommodate the influence of azimuthal anisotropy, both moveout coefficients - the NMO velocity V_{nmo} and the anellipticity parameter η - have to vary with the azimuth α . While $V_{\text{nmo}}(\alpha)$ traces out an ellipse in media of almost any complexity, the form of the function $\eta(\alpha)$ depends on the degree of alignment of the symmetry planes in the constituent layers.

If the azimuths of the vertical symmetry planes do not change from layer to layer, the model as a whole has two orthogonal symmetry planes, and the azimuthal dependence of η [equation 5] is the same as in a homogeneous orthorhombic medium. For purposes of geometrical-spreading correction, such a model is fully equivalent to a single orthorhombic layer. The moveout equation is then controlled by the azimuth ϕ of one of the symmetry planes, two symmetry-plane NMO velocities $V_{\text{nmo}}^{(1,2)}$, and three anellipticity parameters $\eta^{(1,2,3)}$ that govern $\eta(\alpha)$. For media with depth-

varying orientation of the symmetry planes, the accuracy of the moveout equation can be maintained by introducing an additional azimuthal angle ϕ_1 that governs the direction of the “principal axes” of the function $\eta(\alpha)$. The moveout parameters, which serve as the input in the computation of geometrical spreading, are determined using the algorithm of Vasconcelos and Tsvankin based on a 3D nonhyperbolic semblance operator.

Synthetic tests for layered orthorhombic media illustrate the high sensitivity of the spatially varying geometrical spreading to the anisotropic parameters. The magnitude of the anisotropy-induced azimuthal variation of the geometrical spreading may exceed that of the reflection coefficient.¹ Therefore, anisotropic geometrical-spreading correction should be considered an integral part of azimuthal AVO inversion.

The importance of correcting wide-azimuth data for geometrical spreading prior to AVO analysis was highlighted by applying the algorithm to field data acquired at Weyburn field in Canada. The geometrical-spreading factor for the reflection from the top of the fractured reservoir is influenced by the ellipticity of the NMO-velocity function and, especially, by the large values (exceeding 0.2) of the effective parameters $\eta^{(1,2,3)}$. The reliability of the AVO attributes can be improved by taking into account the variation of the geometrical spreading between the symmetry planes (i.e., between the east-west and north-south directions). Note that although information about the effective anisotropy is contained in the input moveout parameters, the difference between the geometrical-spreading factors computed for the top and bottom of a fractured layer can potentially serve as a fracture-detection attribute.

The sensitivity study shows that our geometrical-spreading algorithm is suffi-

¹Comparisons of this type, however, strongly rely on the model assumptions because the geometrical spreading of reflected waves is independent of the elastic parameters beneath the reflector.

ciently robust in the presence of moderate travelttime errors. Still, the results of travelttime fitting and, therefore, geometrical-spreading correction may be somewhat distorted by coherent noise associated, for example, with short-period statics. Also, in the presence of significant amplitude variation with offset and azimuth, it is preferable to estimate the moveout parameters using an AVO-sensitive algorithm.

ACKNOWLEDGMENTS

We are grateful to Ed Jenner (GX Technology) and Tom Davis (CSM) for providing the Weyburn data set to the Center for Wave Phenomena (CWP) and to Ivan Vasconcelos (CSM) for making available his moveout inversion code and processing results. The support for this work was provided by the Consortium Project on Seismic Inverse Methods for Complex Structures at CWP and by the Chemical Sciences, Geosciences and Biosciences Division, Office of Basic Energy Sciences, Office of Science, U.S. Department of Energy.

REFERENCES

- Al-Dajani, A., I. Tsvankin, and M. N. Toksöz, 1998, Nonhyperbolic reflection moveout for azimuthally anisotropic media: 68th Annual International Meeting, SEG, Expanded Abstracts, 1479–1482.
- Alkhalifah, T., and I. Tsvankin, 1995, Velocity analysis for transversely isotropic media: *Geophysics*, **60**, 1550–1566.
- Bakulin, A., V. Grechka, and I. Tsvankin, 2000, Estimation of fracture parameters from reflection seismic data – Part II: Fractured models with orthorhombic symmetry: *Geophysics*, **65**, 1803–1817.
- Cardona, R., 2002, Fluid substitution theories and multicomponent seismic characterization of fractured reservoirs: PhD thesis, Colorado School of Mines.

- Červený, V., 2001, *Seismic ray theory*: Cambridge University Press.
- Gajewski, D., and I. Pšenčík, 1990, Vertical seismic profile synthetics by dynamic ray tracing in laterally varying layered anisotropic structures: *Journal of Geophysical Research*, **95**, 11301–11315.
- Grechka, V., and I. Tsvankin, 1998, 3-D description of normal moveout in anisotropic inhomogeneous media: *Geophysics*, **63**, 1079–1092.
- Grechka, V., and I. Tsvankin, 1999a, 3-D moveout inversion in azimuthally anisotropic media with lateral velocity variation: Theory and a case study: *Geophysics*, **64**, 1202–1218.
- Grechka, V., and I. Tsvankin, 1999b, 3-D moveout velocity analysis and parameter estimation for orthorhombic media: *Geophysics*, **64**, 820–837.
- Hall, S., and J. M. Kendall, 2003, Fracture characterization at Valhall: Application of P-wave amplitude variation with offset and azimuth (AVOA) analysis to a 3-D ocean-bottom data set: *Geophysics*, **68**, 1150–1160.
- Jenner, E., 2001, Azimuthal anisotropy of 3-D compressional wave seismic data, Weyburn field, Saskatchewan, Canada: PhD thesis, Colorado School of Mines.
- Lynn, H.B., D. Campagna, K. M. Simon, and W. E. Beckham, 1999, Relationship of P-wave seismic attributes, azimuthal anisotropy, and commercial gas pay in 3-D P-wave multiazimuth data, Rulison Field, Piceance Basin, Colorado: *Geophysics*, **64**, 1312–1328.
- Mallick, S., K. Craft, and L. Meister, 1998, Determination of the principal directions of azimuthal anisotropy from P-wave seismic data: *Geophysics*, **63**, 692–706.
- Maultzsch, S., S. Horne, S. Archer, and H. Burkhardt, 2003, Effects of an anisotropic overburden on azimuthal amplitude analysis in horizontal transverse isotropic

- media: *Geophysical Prospecting*, **51**, 61–74.
- Pech, A., and I. Tsvankin, 2004, Quartic moveout coefficient for a dipping azimuthally anisotropic layer: *Geophysics*, **69**, 699–707.
- Rüger, A., 2001, Reflection coefficients and azimuthal AVO analysis in anisotropic media: SEG.
- Schoenberg M. and K. Helbig, 1997, Orthorhombic media: Modeling elastic wave behavior in a vertically fractured earth: *Geophysics*, **62**, 1954–1974.
- Tsvankin, I., and L. Thomsen, 1994, Nonhyperbolic reflection moveout in anisotropic media: *Geophysics*, **59**, 1290–1304.
- Tsvankin, I., 1995, Body-wave radiation patterns and AVO in transversely isotropic media: *Geophysics*, **60**, 1409–1425.
- Tsvankin, I., 1997, Anisotropic parameters and P-wave velocity for orthorhombic media: *Geophysics*, **62**, 1292–1309.
- Tsvankin, I., 2005, *Seismic signatures and analysis of reflection data in anisotropic media*: Elsevier Science Publ. Co., Inc (second edition).
- Ursin, B., and K. Hokstad, 2003, Geometrical spreading in a layered transversely isotropic medium with vertical symmetry axis: *Geophysics*, **68**, 2082–2091.
- Vasconcelos, I., and I. Tsvankin, 2004, Inversion of P-wave nonhyperbolic moveout in azimuthally anisotropic media: Methodology and field-data application: 74th Annual International Meeting, SEG, Expanded Abstracts, 171–174 (also submitted to *Geophysical Prospecting*).
- Xu, X., I. Tsvankin, and A. Pech, 2005, Geometrical spreading of P-waves in horizontally layered, azimuthally anisotropic media: *Geophysics*, **70**, D43–D53.

**APPENDIX A—TRAVELTIME DERIVATIVES FOR THE
GEOMETRICAL-SPREADING CORRECTION**

In Appendix B of Paper I the traveltime derivatives needed in the geometrical-spreading equation 1 are expressed through the parameters A_2 , A_4 , and A of the Tsvankin-Thomsen (1994) moveout equation. Here, we showed that an accurate description of traveltimes in layered orthorhombic media can be achieved by using a simpler moveout approximation (equation 4) based on the analogy with vertical transverse isotropy. Equation 4 can be considered as a special case of the Tsvankin-Thomsen moveout equation with the parameters given by

$$A_2(\alpha) = \frac{\sin^2(\alpha - \phi)}{\left(V_{\text{nmo}}^{(1)}\right)^2} + \frac{\cos^2(\alpha - \phi)}{\left(V_{\text{nmo}}^{(2)}\right)^2}, \quad (\text{A-1})$$

$$A_4(\alpha) = -\frac{2\eta(\alpha)}{T_0^2 V_{\text{nmo}}^4(\alpha)}, \quad (\text{A-2})$$

$$A(\alpha) = \frac{1 + 2\eta(\alpha)}{T_0^2 V_{\text{nmo}}^2(\alpha)}, \quad (\text{A-3})$$

where

$$\eta(\alpha) = \eta^{(1)} \sin^2(\alpha - \phi_1) + \eta^{(2)} \cos^2(\alpha - \phi_1) - \eta^{(3)} \sin^2(\alpha - \phi_1) \cos^2(\alpha - \phi_1). \quad (\text{A-4})$$

As discussed in the main text, the azimuth ϕ_1 is equal to ϕ for models with uniform symmetry-plane orientation.

Substituting equations (A-1)–(A-3) into equations (B-2)–(B-4) of Paper I, we obtain the derivatives $\partial T/\partial x$ and $\partial^2 T/\partial x^2$ in terms of the parameters T_0 , ϕ , ϕ_1 , $V_{\text{nmo}}^{(1)}$, $V_{\text{nmo}}^{(2)}$, $\eta^{(1)}$, $\eta^{(2)}$, and $\eta^{(3)}$. The geometrical spreading also depends on the first two traveltime derivatives with respect to the azimuth α , which are expressed in equations (B-5) and (B-6) of Paper I through the corresponding derivatives of A_2 , A_4 , and A . Using equations (A-1)–(A-3) to differentiate A_2 , A_4 , and A with respect to α , we find (prime and double-prime denote the first- and second-order derivatives, respectively)

$$A'_2 = \left[\frac{1}{(V_{\text{nmo}}^{(1)})^2} - \frac{1}{(V_{\text{nmo}}^{(2)})^2} \right] \sin 2(\alpha - \phi), \quad (\text{A-5})$$

$$A''_2 = 2 \left[\frac{1}{(V_{\text{nmo}}^{(1)})^2} - \frac{1}{(V_{\text{nmo}}^{(2)})^2} \right] \cos 2(\alpha - \phi), \quad (\text{A-6})$$

$$\begin{aligned} A'_4 = & \frac{1}{T_0^2 (V_{\text{nmo}}^{(1)})^4 (V_{\text{nmo}}^{(2)})^4} \left\{ 2 \left((V_{\text{nmo}}^{(1)})^2 \cos^2(\alpha - \phi) + (V_{\text{nmo}}^{(2)})^2 \sin^2(\alpha - \phi) \right) \right. \\ & \times \left\{ -\frac{1}{2} \left[(V_{\text{nmo}}^{(1)})^2 + (V_{\text{nmo}}^{(2)})^2 + \left((V_{\text{nmo}}^{(1)})^2 - (V_{\text{nmo}}^{(2)})^2 \right) \cos 2(\alpha - \phi) \right] \right. \\ & \times \left[-\eta^{(1)} + \eta^{(2)} + \eta^{(3)} \cos 2(\alpha - \phi_1) \right] \sin 2(\alpha - \phi_1) \\ & + \left. \left((V_{\text{nmo}}^{(1)})^2 - (V_{\text{nmo}}^{(2)})^2 \right) \cos(\alpha - \phi) \sin(\alpha - \phi) \right. \\ & \left. \times \left[-4\eta^{(2)} \cos^2(\alpha - \phi_1) - 4\eta^{(1)} \sin^2(\alpha - \phi_1) + \eta^{(3)} \sin^2 2(\alpha - \phi_1) \right] \right\} \end{aligned} \quad (\text{A-7})$$

$$\begin{aligned} A''_4 = & \frac{1}{2T_0^2 (V_{\text{nmo}}^{(1)})^4 (V_{\text{nmo}}^{(2)})^4} \left\{ \left((V_{\text{nmo}}^{(1)})^2 - (V_{\text{nmo}}^{(2)})^2 \right) \right. \\ & \times \left[\left((V_{\text{nmo}}^{(1)})^2 + (V_{\text{nmo}}^{(2)})^2 \right) \cos 2(\alpha - \phi) + \left((V_{\text{nmo}}^{(1)})^2 - (V_{\text{nmo}}^{(2)})^2 \right) \cos 4(\alpha - \phi) \right] \\ & \times \left[-4(\eta^{(1)} + \eta^{(2)}) + \eta^{(3)} + 4(\eta^{(1)} - \eta^{(2)}) \cos 2(\alpha - \phi_1) - \eta^{(3)} \cos 4(\alpha - \phi_1) \right] \\ & - 2 \left[(V_{\text{nmo}}^{(1)})^2 + (V_{\text{nmo}}^{(2)})^2 + \left((V_{\text{nmo}}^{(1)})^2 - (V_{\text{nmo}}^{(2)})^2 \right) \cos 2(\alpha - \phi) \right]^2 \\ & \times \left[(\eta^{(2)} - \eta^{(1)}) \cos 2(\alpha - \phi_1) + \eta^{(3)} \cos 4(\alpha - \phi_1) \right] \\ & + 8 \left((V_{\text{nmo}}^{(1)})^2 - (V_{\text{nmo}}^{(2)})^2 \right) \left[(V_{\text{nmo}}^{(1)})^2 + (V_{\text{nmo}}^{(2)})^2 + \left((V_{\text{nmo}}^{(1)})^2 - (V_{\text{nmo}}^{(2)})^2 \right) \cos 2(\alpha - \phi) \right] \\ & \times \left. \left[-\eta^{(1)} + \eta^{(2)} + \eta^{(3)} \cos 2(\alpha - \phi_1) \right] \sin 2(\alpha - \phi) \sin 2(\alpha - \phi_1) \right\}, \quad (\text{A-8}) \end{aligned}$$

$$\begin{aligned}
A' = & -\frac{1}{T_0^2 \left(V_{\text{nmno}}^{(1)}\right)^2 \left(V_{\text{nmno}}^{(2)}\right)^2} \left\{ \left[\left(V_{\text{nmno}}^{(1)}\right)^2 + \left(V_{\text{nmno}}^{(2)}\right)^2 + \left(\left(V_{\text{nmno}}^{(1)}\right)^2 - \left(V_{\text{nmno}}^{(2)}\right)^2\right) \cos 2(\alpha - \phi) \right] \right. \\
& \times \left[-\eta^{(1)} + \eta^{(2)} + \eta^{(3)} \cos 2(\alpha - \phi_1) \right] \sin 2(\alpha - \phi_1) \\
& + \left(\left(V_{\text{nmno}}^{(1)}\right)^2 - \left(V_{\text{nmno}}^{(2)}\right)^2 \right) \cos(\alpha - \phi) \sin(\alpha - \phi) \\
& \left. \times \left[2 + 4\eta^{(2)} \cos^2(\alpha - \phi_1) + 4\eta^{(1)} \sin^2(\alpha - \phi_1) - \eta^{(3)} \sin^2 2(\alpha - \phi_1) \right] \right\}, \quad (\text{A-9})
\end{aligned}$$

$$\begin{aligned}
A'' = & \frac{1}{T_0^2 \left(V_{\text{nmno}}^{(1)}\right)^2 \left(V_{\text{nmno}}^{(2)}\right)^2} \left\{ \frac{1}{2} \left(\left(V_{\text{nmno}}^{(1)}\right)^2 - \left(V_{\text{nmno}}^{(2)}\right)^2 \right) \cos 2(\alpha - \phi) \right. \\
& \times \left[-4(1 + \eta^{(1)} + \eta^{(2)}) + \eta^{(3)} + 8(\eta^{(1)} - \eta^{(2)}) \cos 2(\alpha - \phi_1) - 5\eta^{(3)} \cos 4(\alpha - \phi_1) \right] \\
& + 2 \left(\left(V_{\text{nmno}}^{(1)}\right)^2 + \left(V_{\text{nmno}}^{(2)}\right)^2 \right) \left[(\eta^{(1)} - \eta^{(2)}) \cos 2(\alpha - \phi_1) - \eta^{(3)} \cos 4(\alpha - \phi_1) \right] \\
& \left. + 4 \left(\left(V_{\text{nmno}}^{(1)}\right)^2 - \left(V_{\text{nmno}}^{(2)}\right)^2 \right) \left[-\eta^{(1)} + \eta^{(2)} + \eta^{(3)} \cos 2(\alpha - \phi_1) \right] \sin 2\alpha \sin 2(\alpha - \phi_1) \right\} \quad (0)
\end{aligned}$$

Substitution of equations (A-5)–(A-10) into equations (B-5) and (B-6) of Paper I yields the derivatives $\partial T/\partial\alpha$ and $\partial^2 T/\partial\alpha^2$ as explicit functions of the moveout parameters.

TABLES

	Symmetry type	V_{P0} (km/s)	Thickness (km)	$V_{\text{nmo}}^{(1)}$	$V_{\text{nmo}}^{(2)}$	$\eta^{(1)}$	$\eta^{(2)}$	$\eta^{(3)}$
Layer 1	ISO	1.5	0.2	1.5	1.5	0	0	0
Layer 2	ORTH	2.437	0.9	2.632	2.239	0.211	0.398	0.194
Layer 3	ORTH	3.0	0.9	3.146	2.683	0.182	0.313	-0.056
Layer 4	ISO	3.2	0.5	3.2	3.2	0	0	0

TABLE 1. Parameters of a four-layer model (model 1) that includes two orthorhombic layers with aligned vertical symmetry planes $\phi = 0^\circ$ and $\phi = 90^\circ$. The density used in the computation of the reflection coefficient in Figure 8 is set to 1.0 g/cm^3 in all layers.

	Symmetry type	V_{P0} (km/s)	Thickness (km)	$V_{\text{nmo}}^{(1)}$	$V_{\text{nmo}}^{(2)}$	$\eta^{(1)}$	$\eta^{(2)}$	$\eta^{(3)}$
Layer 1	ORTH	3.0	1.0	2.509	2.683	0.857	0.875	-0.192
Layer 2	ORTH	3.0	1.0	3.421	2.509	0.038	1.071	0.030

TABLE 2. Parameters of a model (model 2) that includes two orthorhombic layers with misaligned symmetry planes and uncommonly strong anisotropy. The azimuth of the $[x_1, x_3]$ symmetry plane is $\phi = 45^\circ$ in layer 1 and $\phi = 0^\circ$ in layer 2.

FIGURES

FIG. 1. Accuracy of equation 4 in describing full-azimuth, long-offset P-wave moveout in a homogeneous orthorhombic layer. The moveout parameters are found by fitting equation 4 to traveltimes computed by anisotropic ray tracing. The map shows the difference between the best-fit and ray-traced traveltimes normalized by the zero-offset time (0.82 s). The radius corresponds to the source-receiver offset (the maximum offset-to-depth ratio is three), the numbers around the perimeter indicate the azimuth with respect to the $[x_1, x_3]$ symmetry plane. The P-wave velocity parameters of the model are $V_{P0} = 2.437$ km/s, $\epsilon^{(1)} = 0.329$, $\epsilon^{(2)} = 0.258$, $\delta^{(1)} = 0.083$, $\delta^{(2)} = -0.078$, and $\delta^{(3)} = -0.106$. The corresponding moveout parameters are $V_{\text{nmo}}^{(1)} = 2.632$ km/s, $V_{\text{nmo}}^{(2)} = 2.239$ km/s, $\eta^{(1)} = 0.211$, $\eta^{(2)} = 0.398$, and $\eta^{(3)} = 0.194$.

FIG. 2. Accuracy of equation 4 for the layered azimuthally anisotropic model from Table 1 (model 1). The azimuths ($\alpha = 0^\circ$, 45° , and 90°) with respect to the $[x_1, x_3]$ symmetry plane are marked on the plot. The dashed line is the ray-traced traveltime for the reflection from the bottom of layer 3, the solid line is the corresponding traveltime computed from equation 4 with the following estimated (best-fit) moveout parameters: $\phi = 90^\circ$, $V_{\text{nmo}}^{(1)} = 2.307$ km/s, $V_{\text{nmo}}^{(2)} = 2.675$ km/s, $\eta^{(1)} = 0.305$, $\eta^{(2)} = 0.222$, and $\eta^{(3)} = -0.006$.

FIG. 3. Map of the traveltime residuals (normalized by the zero-offset time $T_0 = 1.334$ s) plotted as a function of offset and azimuth for the two-layer model with misaligned symmetry planes from Table 2 (model 2). The residuals are computed for the reflection from the bottom of the model as the differences between the best-fit traveltimes from equation 4 and ray tracing. The maximum offset is 4 km; the corresponding offset-to-depth ratio is two. The estimated moveout parameters are $\phi = 78^\circ$, $V_{\text{nmo}}^{(1)} = 2.60$ km/s, $V_{\text{nmo}}^{(2)} = 3.00$ km/s, $\eta^{(1)} = 0.567$, $\eta^{(2)} = 0.330$, and $\eta^{(3)} = 0.104$.

FIG. 4. Comparison of the effective parameter $\eta(\alpha)$ computed from the VTI averaging equation 6 (solid curve) and estimated by the moveout-inversion algorithm (dashed). The model is composed of two orthorhombic layers; for the top layer, $\phi = 15^\circ$, $V_{\text{nm}o}^{(1)} = 2.236$ km/s, $V_{\text{nm}o}^{(2)} = 2.850$ km/s, $\eta^{(1)} = 0.375$, $\eta^{(2)} = 0.000$, and $\eta^{(3)} = -0.086$; for the bottom layer, $\phi = 0^\circ$, $V_{\text{nm}o}^{(1)} = 3.421$ km/s, $V_{\text{nm}o}^{(2)} = 2.683$ km/s, $\eta^{(1)} = 0.000$, $\eta^{(2)} = 0.375$, and $\eta^{(3)} = 0.163$. The maximum offset-to-depth ratio of the data used in the inversion is two.

FIG. 5. Same as Figure 3, but the moveout parameters of equation 4 were estimated by the modified inversion algorithm that allows for an independent orientation of the $\eta(\alpha)$ -curve [equation 7]. The best-fit parameters are $\phi = 81^\circ$, $V_{\text{nm}o}^{(1)} = 2.586$ km/s, $V_{\text{nm}o}^{(2)} = 3.00$ km/s, $\eta^{(1)} = 0.594$, $\eta^{(2)} = 0.339$, $\eta^{(3)} = 0.161$, and $\phi_1 = 89^\circ$.

FIG. 6. Map of the geometrical spreading for the reflection from the bottom of layer 3 in model 1 (Table 1). The factor L is normalized by its value in the reference isotropic homogeneous medium with the velocity equal to $V_{\text{nm}o} = (V_{\text{nm}o}^{(1)} + V_{\text{nm}o}^{(2)})/2$. The maximum offset-to-depth ratio is two.

FIG. 7. Azimuthally varying geometrical spreading for model 1 (Figure 6) computed for an offset of 2 km. The corresponding phase incidence angle at the reflector (the bottom of layer 3) is close to 30° ($30^\circ \pm 5^\circ$).

FIG. 8. Azimuthally varying reflection coefficient from the bottom of layer 3 in model 1 (Table 1) computed for the phase incidence angle at the reflector equal to 30° .

FIG. 9. Accuracy of our method for the reflection from the bottom of layer 3 in model 1; the azimuths from the $[x_1, x_3]$ symmetry plane are $\alpha = 0^\circ$, 40° , and 90° .

The geometrical-spreading factor L computed by our algorithm (solid lines) is compared with the output of dynamic ray-tracing code ANRAY (dashed).

FIG. 10. Percentage error of the geometrical spreading for model 1 (Figure 6) caused by the traveltime error function $4 \sin(3\pi x/x_{\max}) \sin 4\alpha$ (in ms). The maximum offset-to-depth ratio is two.

FIG. 11. Histogram of the error distribution in the geometrical spreading computed in the $[x_1, x_3]$ symmetry plane of model 1 (Figure 6). The moveout parameters were contaminated by Gaussian noise with the following standard deviations: 0.5% for T_0 , 3% for $V_{\text{nmo}}^{(1)}$ and $V_{\text{nmo}}^{(2)}$, 30% for $\eta^{(1)}$ and $\eta^{(2)}$, and 50% for $\eta^{(3)}$. The offset-to-depth ratio is equal to one (a) and two (b). The standard deviation of the error in L is 5% in plot (a) and 8% in plot (b).

FIG. 12. Map of the geometrical spreading for the P-wave reflection from the Mississippian formation (the top of the reservoir) at Weyburn field computed for CMP 10829. The factor L is normalized by its value in the reference isotropic homogeneous medium with the velocity equal to $(V_{\text{nmo}}^{(1)} + V_{\text{nmo}}^{(2)})/2$. The moveout parameters are taken from Vasconcelos and Tsvankin (2004): $\phi = 99^\circ$, $V_{\text{nmo}}^{(1)} = 2.371$ km/s, $V_{\text{nmo}}^{(2)} = 2.464$ km/s, $\eta^{(1)} = 0.255$, $\eta^{(2)} = 0.186$, and $\eta^{(3)} = -0.062$. The reflector depth is 1.4 km (the maximum offset-to-depth ratio is 2.5). The North-South direction is at $\phi = 0^\circ$, and the East-West at $\phi = 90^\circ$.

FIG. 13. Normalized geometrical spreading from Figure 12 in the east-west and north-south directions.

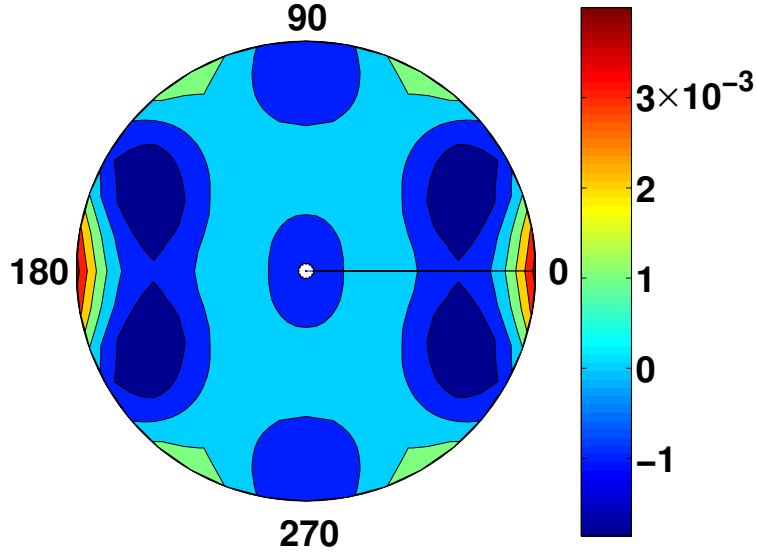


FIG. 1. Accuracy of equation 4 in describing full-azimuth, long-offset P-wave moveout in a homogeneous orthorhombic layer. The moveout parameters are found by fitting equation 4 to traveltimes computed by anisotropic ray tracing. The map shows the difference between the best-fit and ray-traced traveltimes normalized by the zero-offset time (0.82 s). The radius corresponds to the source-receiver offset (the maximum offset-to-depth ratio is three), the numbers around the perimeter indicate the azimuth with respect to the $[x_1, x_3]$ symmetry plane. The P-wave velocity parameters of the model are $V_{P0} = 2.437$ km/s, $\epsilon^{(1)} = 0.329$, $\epsilon^{(2)} = 0.258$, $\delta^{(1)} = 0.083$, $\delta^{(2)} = -0.078$, and $\delta^{(3)} = -0.106$. The corresponding moveout parameters are $V_{\text{nmo}}^{(1)} = 2.632$ km/s, $V_{\text{nmo}}^{(2)} = 2.239$ km/s, $\eta^{(1)} = 0.211$, $\eta^{(2)} = 0.398$, and $\eta^{(3)} = 0.194$.

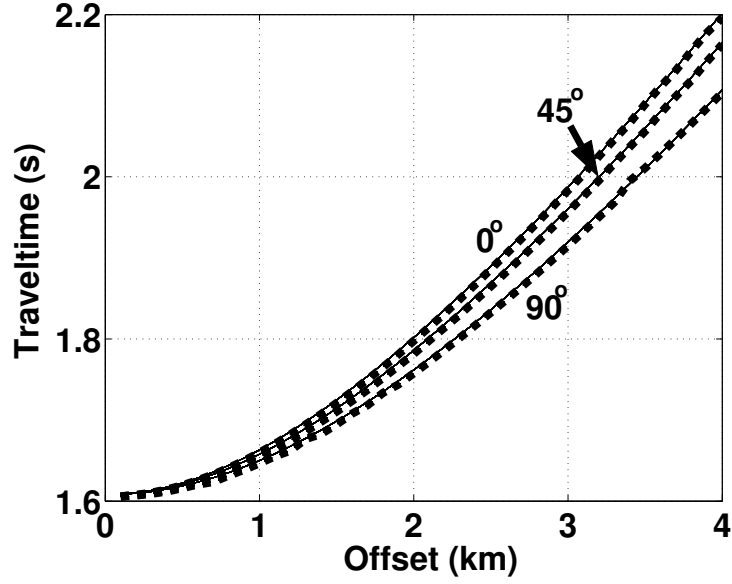


FIG. 2. Accuracy of equation 4 for the layered azimuthally anisotropic model from Table 1 (model 1). The azimuths ($\alpha = 0^\circ, 45^\circ,$ and 90°) with respect to the $[x_1, x_3]$ symmetry plane are marked on the plot. The dashed line is the ray-traced traveltime for the reflection from the bottom of layer 3, the solid line is the corresponding traveltime computed from equation 4 with the following estimated (best-fit) moveout parameters: $\phi = 90^\circ$, $V_{\text{nmo}}^{(1)} = 2.307$ km/s, $V_{\text{nmo}}^{(2)} = 2.675$ km/s, $\eta^{(1)} = 0.305$, $\eta^{(2)} = 0.222$, and $\eta^{(3)} = -0.006$.

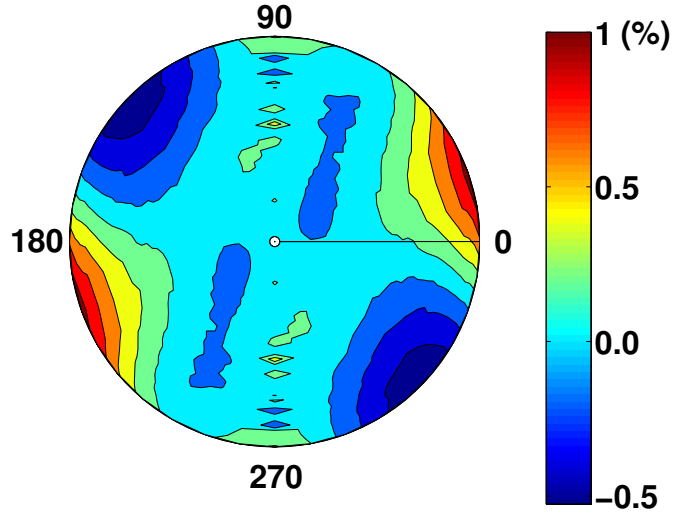


FIG. 3. Map of the traveltime residuals (normalized by the zero-offset time $T_0 = 1.334$ s) plotted as a function of offset and azimuth for the two-layer model with misaligned symmetry planes from Table 2 (model 2). The residuals are computed for the reflection from the bottom of the model as the differences between the best-fit traveltimes from equation 4 and ray tracing. The maximum offset is 4 km; the corresponding offset-to-depth ratio is two. The estimated moveout parameters are $\phi = 78^\circ$, $V_{\text{nmo}}^{(1)} = 2.60$ km/s, $V_{\text{nmo}}^{(2)} = 3.00$ km/s, $\eta^{(1)} = 0.567$, $\eta^{(2)} = 0.330$, and $\eta^{(3)} = 0.104$.

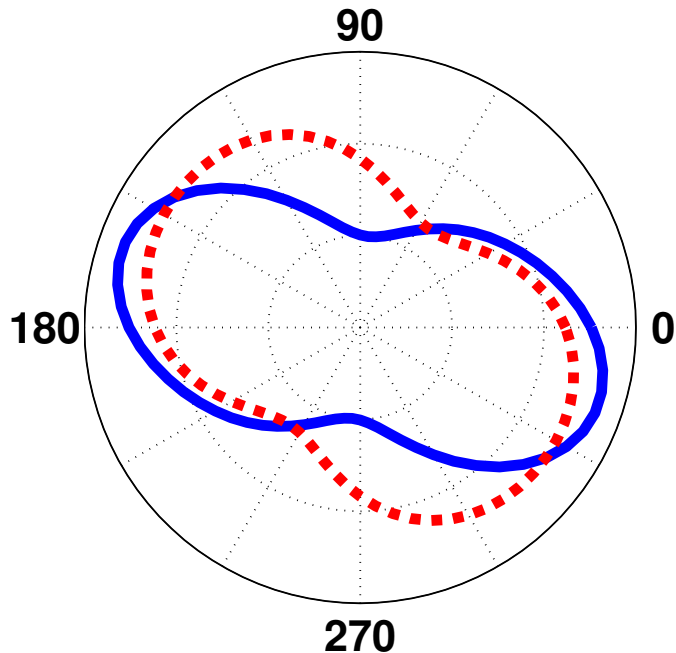


FIG. 4. Comparison of the effective parameter $\eta(\alpha)$ computed from the VTI averaging equation 6 (solid curve) and estimated by the moveout-inversion algorithm (dashed). The model is composed of two orthorhombic layers; for the top layer, $\phi = 15^\circ$, $V_{\text{nmo}}^{(1)} = 2.236$ km/s, $V_{\text{nmo}}^{(2)} = 2.850$ km/s, $\eta^{(1)} = 0.375$, $\eta^{(2)} = 0.000$, and $\eta^{(3)} = -0.086$; for the bottom layer, $\phi = 0^\circ$, $V_{\text{nmo}}^{(1)} = 3.421$ km/s, $V_{\text{nmo}}^{(2)} = 2.683$ km/s, $\eta^{(1)} = 0.000$, $\eta^{(2)} = 0.375$, and $\eta^{(3)} = 0.163$. The maximum offset-to-depth ratio of the data used in the inversion is two.

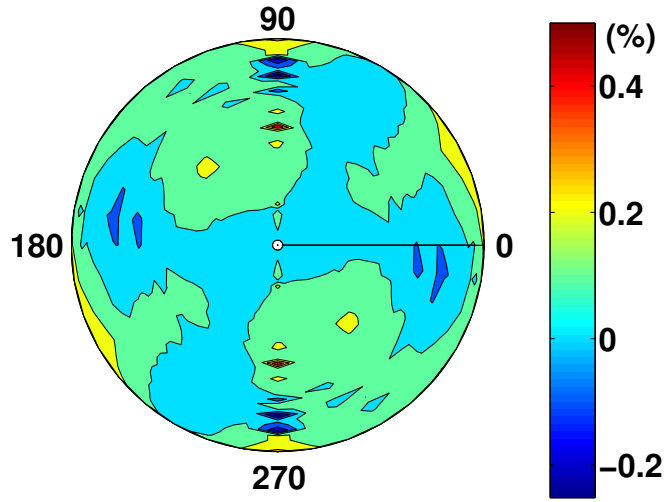


FIG. 5. Same as Figure 3, but the moveout parameters of equation 4 were estimated by the modified inversion algorithm that allows for an independent orientation of the $\eta(\alpha)$ -curve [equation 7]. The best-fit parameters are $\phi = 81^\circ$, $V_{\text{nmo}}^{(1)} = 2.586$ km/s, $V_{\text{nmo}}^{(2)} = 3.00$ km/s, $\eta^{(1)} = 0.594$, $\eta^{(2)} = 0.339$, $\eta^{(3)} = 0.161$, and $\phi_1 = 89^\circ$.

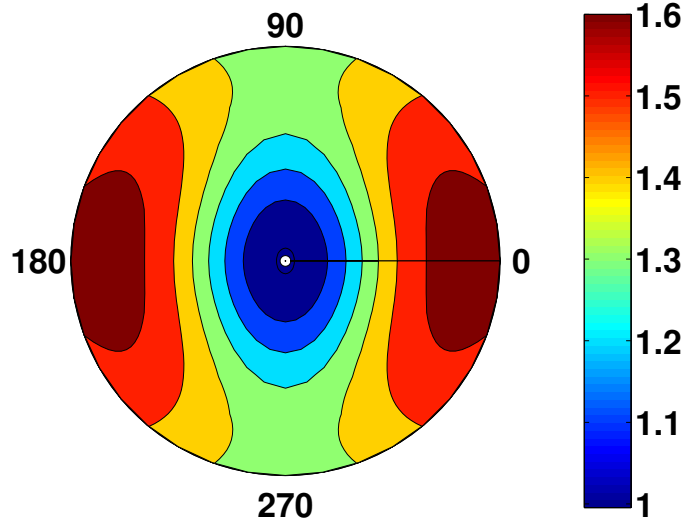


FIG. 6. Map of the geometrical spreading for the reflection from the bottom of layer 3 in model 1 (Table 1). The factor L is normalized by its value in the reference isotropic homogeneous medium with the velocity equal to $V_{\text{nmo}} = (V_{\text{nmo}}^{(1)} + V_{\text{nmo}}^{(2)})/2$. The maximum offset-to-depth ratio is two.

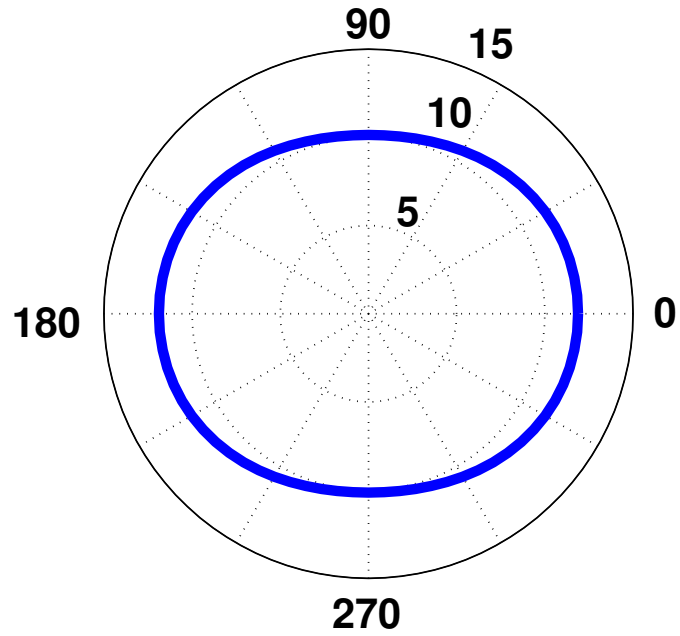


FIG. 7. Azimuthally varying geometrical spreading for model 1 (Figure 6) computed for an offset of 2 km. The corresponding phase incidence angle at the reflector (the bottom of layer 3) is close to 30° ($30^\circ \pm 5^\circ$).

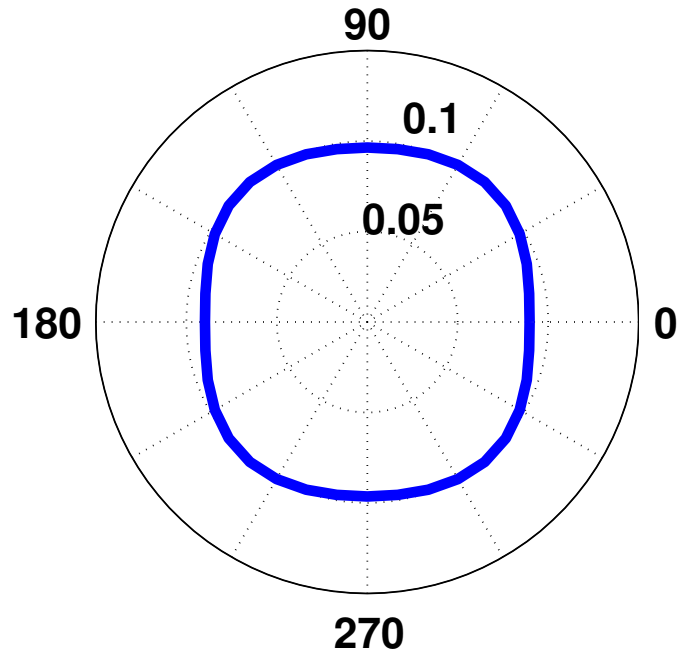


FIG. 8. Azimuthally varying reflection coefficient from the bottom of layer 3 in model 1 (Table 1) computed for the phase incidence angle at the reflector equal to 30° .

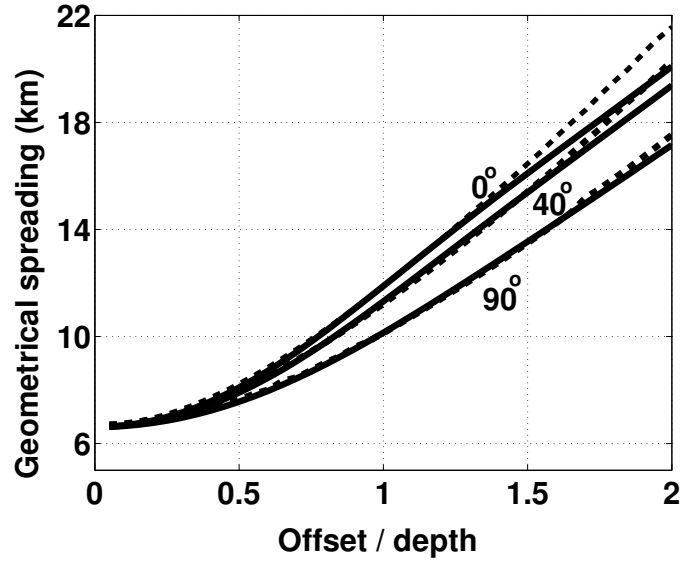


FIG. 9. Accuracy of our method for the reflection from the bottom of layer 3 in model 1; the azimuths from the $[x_1, x_3]$ symmetry plane are $\alpha = 0^\circ$, 40° , and 90° . The geometrical-spreading factor L computed by our algorithm (solid lines) is compared with the output of dynamic ray-tracing code ANRAY (dashed).

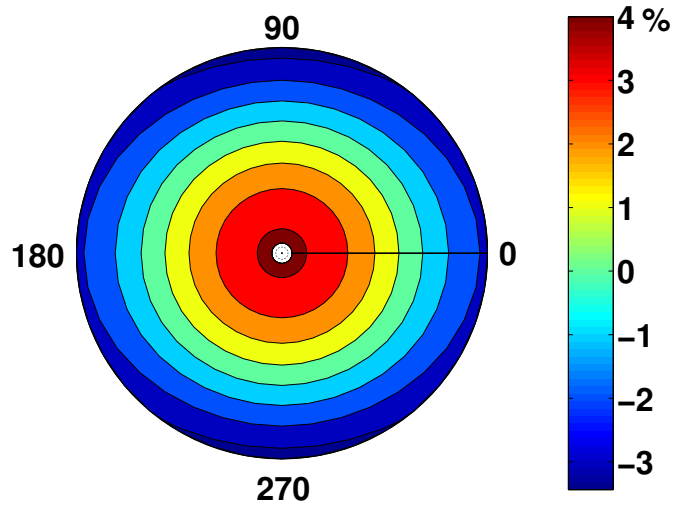


FIG. 10. Percentage error of the geometrical spreading for model 1 (Figure 6) caused by the traveltime error function $4 \sin(3\pi x/x_{\max}) \sin 4\alpha$ (in ms). The maximum offset-to-depth ratio is two.

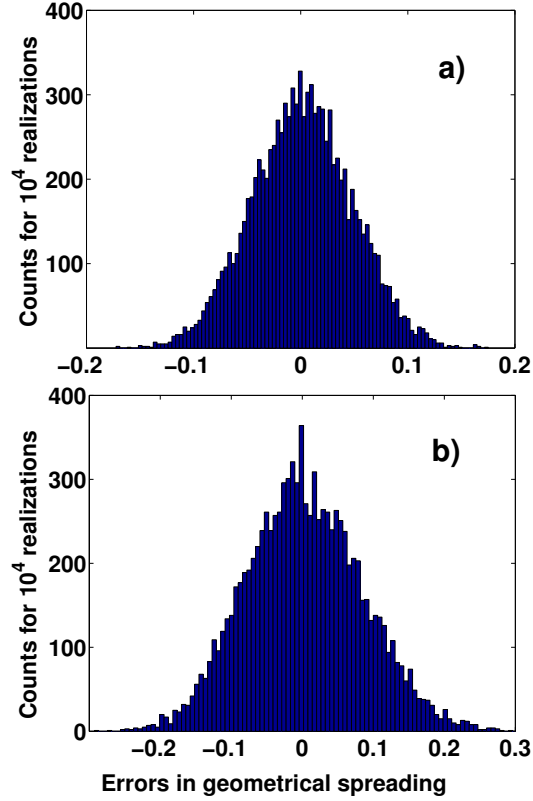


FIG. 11. Histogram of the error distribution in the geometrical spreading computed in the $[x_1, x_3]$ symmetry plane of model 1 (Figure 6). The moveout parameters were contaminated by Gaussian noise with the following standard deviations: 0.5% for T_0 , 3% for $V_{\text{nmo}}^{(1)}$ and $V_{\text{nmo}}^{(2)}$, 30% for $\eta^{(1)}$ and $\eta^{(2)}$, and 50% for $\eta^{(3)}$. The offset-to-depth ratio is equal to one (a) and two (b). The standard deviation of the error in L is 5% in plot (a) and 8% in plot (b).

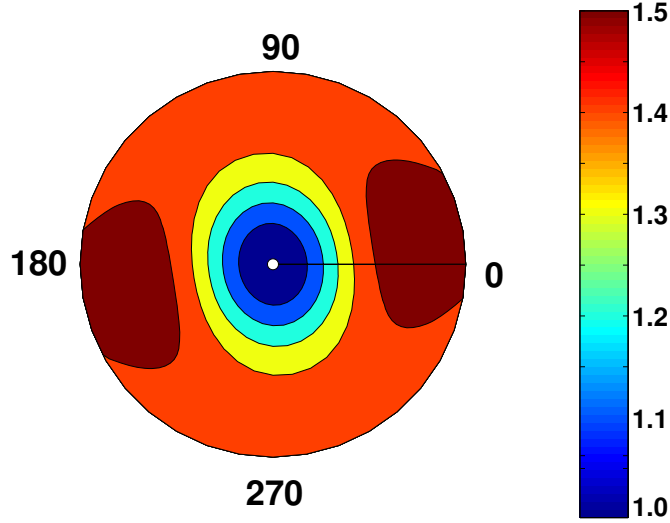


FIG. 12. Map of the geometrical spreading for the P-wave reflection from the Mississippian formation (the top of the reservoir) at Weyburn field computed for CMP 10829. The factor L is normalized by its value in the reference isotropic homogeneous medium with the velocity equal to $(V_{\text{nmo}}^{(1)} + V_{\text{nmo}}^{(2)})/2$. The moveout parameters are taken from Vasconcelos and Tsvankin (2004): $\phi = 99^\circ$, $V_{\text{nmo}}^{(1)} = 2.371$ km/s, $V_{\text{nmo}}^{(2)} = 2.464$ km/s, $\eta^{(1)} = 0.255$, $\eta^{(2)} = 0.186$, and $\eta^{(3)} = -0.062$. The reflector depth is 1.4 km (the maximum offset-to-depth ratio is 2.5). The North-South direction is at $\phi = 0^\circ$, and the East-West at $\phi = 90^\circ$.

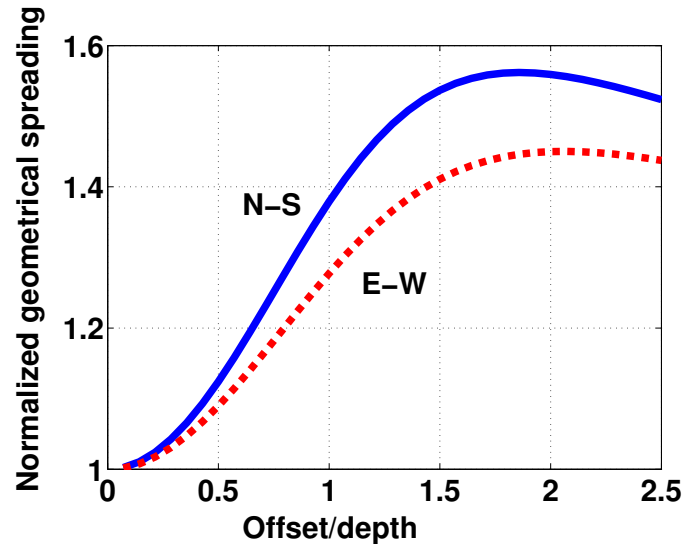


FIG. 13. Normalized geometrical spreading from Figure 12 in the east-west and north-south directions.